

Verification of experimental saltwater intrusion interface in unconfined coastal aquifers using numerical and analytical solutions

Verifica dell'interfaccia tra acque dolci e acque di intrusione salina in acquiferi costieri non confinati utilizzando soluzioni numeriche e analitiche

Sobhy R. EMARA ^a , Asaad M. ARMANUOS ^a, Tamer A. GADO ^a, Bakenaz A. ZEIDAN ^a

^a Irrigation and Hydraulics Engineering Department, Faculty of Engineering, Tanta University, Tanta, Egypt

Email  : sobhy_emara39@f-eng.tanta.edu.eg; email: asaad.matter@f-eng.tanta.edu.eg; tamer.gado@f-eng.tanta.edu.eg; b.zeidan@f-eng.tanta.edu.eg

ARTICLE INFO

Ricevuto/Received: 31 March 2023

Accettato/Accepted: 8 June 2023

Pubblicato online/Published online:

30 September 2023

Handling Editor:

Giovanna De Filippis

Citation:

Emara, SR., Armanuos, AM., Gado, TA., Zeidan, BA. (2023). Verification of experimental saltwater intrusion interface in unconfined coastal aquifers using numerical and analytical solutions. *Acque Sotteranee - Italian Journal of Groundwater*, 12(3), 23- 38
<https://doi.org/10.7343/as-2023-668>

Correspondence to:

Sobhy R. Emara 

sobhy_emara39@f-eng.tanta.edu.eg

Keywords: Saltwater Intrusion, Numerical Simulation, Experimental Modeling, Sandbox Model, Sea Level Rise, SEAWAT.

Parole chiave: Intrusione salina, Simulazione numerica, Modellazione sperimentale, Modello sperimentale con sabbia, Innalzamento del livello del mare, SEAWAT.

Copyright: © 2023 by the authors. License Associazione Acque Sotteranee. This is an open access article under the CC BY-NC-ND license: <http://creativecommons.org/licenses/by-nc-nd/4.0/>

Riassunto

L'intrusione salina è un problema ambientale diffuso che rappresenta una minaccia per gli acquiferi costieri. Per affrontare questo problema, questo studio utilizza metodi sia numerici che sperimentali per analizzare il fenomeno dell'intrusione salina in funzione dell'innalzamento del livello del mare e di diverse condizioni al contorno di carico idraulico dell'acquifero nel caso di due acquiferi omogenei. Lo studio confronta i carichi idraulici calcolati numericamente in condizioni transitorie con i risultati sperimentali relativi alle concentrazioni saline nel caso di cuneo salino in ritirata e in avanzamento. Nell'acquifero a bassa permeabilità, l'errore quadratico medio è pari a 0,33 cm ed R^2 è maggiore di 0,9817. Analogamente, nell'acquifero ad alta permeabilità, l'errore quadratico medio è pari a 0,92 cm ed R^2 è maggiore di 0,9335. Lo studio confronta anche i risultati di dieci test sperimentali relativi all'avanzamento del cuneo di intrusione salina in condizioni stazionarie con sette diverse soluzioni analitiche. I risultati sperimentali vengono quindi confrontati con queste soluzioni analitiche per trovare l'equazione più adatta. L'equazione di Rumer e Harleman mostra un buon accordo con il cuneo sperimentale di intrusione salina, mentre l'equazione di Anderson si adatta bene per il calcolo della distanza alla quale l'interfaccia acqua dolce-acqua salata interseca il fondo impermeabile dell'acquifero. Nel complesso, questo studio fornisce preziose informazioni sul fenomeno dell'intrusione salina negli acquiferi costieri e i risultati possono essere utilizzati per indirizzare le strategie di gestione e mitigare gli impatti negativi dell'intrusione salina. Lo studio ha fatto luce su come il carico idraulico dell'acquifero e l'innalzamento del livello del mare influenzano la dinamica dell'interfaccia acqua dolce-acqua salata.

Abstract

Saltwater intrusion (SWI) is a widespread environmental problem that poses a threat to coastal aquifers. To address this issue, this research employs both numerical and experimental methods to study saltwater intrusion under the impact of sea level rise and varying freshwater boundary conditions in two homogeneous aquifers. The study compares transient numerical groundwater heads and salt concentrations to experimental results under receding-front and advancing front conditions. In the low permeability aquifer, the root mean square error is 0.33 cm and the R^2 is greater than 0.9817. Similarly, in the high permeability aquifer, the root mean square error is 0.92 cm and the R^2 is greater than 0.9335. The study also compares the results of ten experimental tests for steady-state saltwater intrusion wedge and toe length with seven different analytical solutions. The experimental results are then compared to these analytical solutions to find the most suitable equation. The Rumer and Harleman equation shows good agreement with experimental saltwater intrusion wedge, while the Anderson equation is a good fit for saltwater intrusion toe length. Overall, this research provides valuable insights into saltwater intrusion in coastal aquifers, and the findings can be used to inform policies and management strategies to mitigate the negative impacts of saltwater intrusion. The investigation shed light on how inland water head and Sea Level Rise (SLR) affect SWI behavior.

Introduction

Seawater intrusion (SWI) is a major problem for coastal habitats in many regions around the world, particularly when groundwater resources are the primary source of freshwater supplies. Salinity intrusion into groundwater aquifers is typically avoided by ambient groundwater that discharges toward the sea. In general, the severe effects of SWI are due to excessive groundwater abstraction lowering groundwater heads and reducing freshwater discharge (Werner et al., 2013). Climate change is one of the main factors that adversely affect saltwater intrusion on several levels. There is a direct effect represented by Sea Level Rise (SLR) and an indirect effect, represented by the scarcity of rain in some areas, and consequently a decrease in the natural recharge (drought). These effects lead to an extension of saltwater wedge inland, which is exacerbated by the excessive withdrawal of groundwater (Ketabchi et al., 2016; Abdoulhalik & Ahmed, 2017).

In a sloping coastal unconfined aquifer with a constant recharge rate and the SWI sharp-interface assumption, Koussis et al. (2012) derived steady-state analytical solutions for the location of the interface toe. Lu et al. (2015) derived analytical solutions for SWI in both unconfined and confined coastal aquifers with an inland general-head boundary condition. Then the distance of interface toe movement in response to a 1 m SLR was predicted using the developed solutions. Then, using the developed solutions, the saltwater wedge toe movement, when subjected to a 1 m SLR, was estimated. Lu et al. (2016) obtained steady-state analytical solutions for SWI in sloping unconfined and confined aquifers assuming sharp-interface SWI.

In an anisotropic aquifer of defined depth, Anderson (2021) derived an analytical solution for unconfined coastal interface discharge. Luo et al. (2022) derived analytical solutions for the steady-state SWI in unconfined coastal aquifers, based on the sharp-interface assumption. The discharge equation was solved analytically while considering unsaturated flow.

Saltwater intrusion caused by SLR is one of the major threats to freshwater resources in the world presently (Shi et al., 2018; Vu et al., 2018; Abd-Elhamid et al., 2020; Song et al., 2020; Dang et al., 2020). When it comes to modeling seawater intrusion, analytical solutions (Ketabchi et al., 2014; Lu et al., 2016) and numerical modeling (Gossel et al., 2010; Sherif et al., 2014; Mehdizadeh et al., 2017; Abd-Elaty & Zelenakova, 2022) are viable options.

Zheng et al. (2021) were the pioneers in uncovering how saltwater can be effectively removed in the presence of subsurface dams. They also investigated how the structure of the dam and the characteristics of the aquifer affect the efficiency of removing saltwater that remains upstream of the dam. The researchers demonstrated that when there are high-concentration gradients, a crucial mechanism for saltwater removal involves the lower-concentration mixing zone. This zone serves as a significant pathway through which saltwater can flow over the subsurface dam and reach the saltwater edge.

This sheds light on the ongoing dissemination of saltwater and its movement towards the edge of the aquifer.

The study conducted by Fang et al. (2022) focused on investigating the impact of transient external forcing conditions on the stability of a phenomenon called tide-induced upper saline plume (USP). The USP refers to a seasonal subsurface inflow that occurs in coastal aquifers. The research involved both experimental and numerical analysis to better comprehend the behavior of the USP under varying conditions. The results indicated that the USP exhibited a rapid response to fluctuations in seasonal subsurface inflow, causing it to expand into the intertidal zone. This expansion into the intertidal zone means a significant dynamic transformation process. The study also revealed that the frequency contrast between the seasonal subsurface inflow and the tide played a crucial role in influencing the dynamic transformation process occurring in the intertidal region. Specifically, an inverse relationship was observed between the frequency contrast and the duration of the unstable flow. In other words, when the frequency contrast between the seasonal subsurface inflow and tide was higher, the duration of the unstable flow decreased.

Chang et al. (2011) demonstrated how both confined and unconfined aquifers could be impacted by changes in freshwater discharges increasing sea levels and increasing sea levels. Kuan et al. (2012) discussed how variations in regional freshwater inflow and tide patterns can influence SWI in coastal aquifers. Goswami & Clement (2007) established a benchmark model for seawater intrusion problems using laboratory-scale experiments. They investigated the saltwater wedge's advancing and retreating motion in steady-state and transient scenarios. More recently, Abdoulhalik & Ahmed (2018) demonstrated that the advancing saltwater wedge required roughly twice as long to attain a steady-state equilibrium than the receding wedge.

Therefore, proper management and understanding of coastal aquifers are crucial components of global water security. Comprehensive numerical models, such as SUTRA (Voss & Koch, 2001), SEAWAT (Guo & Langevin, 2002), and FEFLOW (Diersch, 2013), have been developed to simulate the SWI under various conditions (Armanuos et al., 2019, 2020a, 2020b; Guo et al., 2020; Gao et al., 2021; Abdoulhalik et al., 2021).

The goal of the current research was to study the impact of inland boundary conditions on SWI caused by SLR in coastal aquifers under both transient and steady-state conditions. The numerical model SEAWAT was applied for validation purposes. A comparison between the steady-state saltwater wedges and the analytical solutions developed by Ghyben (1888), Glover (1959), Rumer Jr & Harleman (1963), Verruijt (1968), and Kashef (1983) was conducted. Also, the steady-state saltwater intrusion toe length results from ten experimental tests were compared with the analytical solutions developed by Lu et al. (2015) and Anderson (2021) to identify the most suitable equation.

Methodology and modeling

To study the influence of variable-head inland boundary and SLR on the SWI process, two different scenarios were studied in two distinct homogeneous aquifers. For scenario 1, the saltwater level was fixed, and the inland fresh groundwater head was raised. Then, under scenario 2, the inland groundwater head was fixed, and the saltwater level was increased. During the experiments, for the studied aquifers, the saltwater-freshwater reached five steady-state conditions. First, the salt transfer in the aquifers was detected throughout the experiments. Then, SEAWAT was used in this study to construct numerical models of salt transport in groundwater flow to explore the effect of SLR in the investigated unconfined aquifers. Finally, the steady-state saltwater wedges were compared with the analytical solutions developed by Ghyben (1888), Glover (1959), Rumer Jr & Harleman (1963), Verruijt (1968), and Kashef (1983).

Experimental Methods

Simulating the behavior and impact of saltwater intrusion has long been done using scaled-down or physical models. (Christensen & JR, 1974; Brakefield, 2008; Luyun Jr et al., 2011; Werner et al., 2013; Armanuos et al., 2019; Hussain et al., 2019). These are useful tools for studying and visualizing the interactions between fluids with varying properties in the same domain. Physical model simulation observations have been frequently utilized to compare with or validate numerical simulations (Sriapai et al., 2012).

The experiments were carried out in a laboratory sandbox tank measuring 114 cm (length) x 28 cm (height) x 8 cm

(width) and replicating a cross-section of an unconfined coastal aquifer (Fig. 1). From left to right, the tank was separated into three sections: a freshwater reservoir with a length of 12 cm, a porous media chamber with a length of 90 cm, and a saltwater reservoir with a length of 12 cm. A layer of fine mesh screen was placed to separate the reservoirs, enabling water to flow through but obstructing the porous medium.

To represent the unconfined coastal aquifer in the sandbox model, silica sands of mean diameter 1700 μm and 1180 μm were utilized as the aquifer medium. Under saturated conditions, the silica sand was compressed in consecutive even-sized layers to prevent air bubbles from maintaining in the sand pores. The sand was well mixed during packing and softly compressed after packing (Abdoulhalik et al., 2017; Gao et al., 2021). Clamps were employed during sand packing to restrict expansion and keep the sand tank's width unchanged (Armanuos et al., 2019). The study evaluated two different homogenous aquifers namely: high K and low K. The high K aquifer was conducted with sand with a mean diameter of 1700 μm and the low K aquifer with sand with a mean diameter of 1180 μm . The porous media longitudinal dispersivity (α_L) was set to be equal to 0.15 cm, a common value in laboratory-scale studies (Abarca & Clement, 2009; Sun et al., 2019; Chang et al., 2020; Armanuos et al., 2020a). The transverse dispersivity (α_T) was set to be 10% of α_L , as same as in prior research (Walther et al., 2017; Armanuos et al., 2019).

Freshwater was obtained by using tap water. Before the experiments, 150 liters of the saltwater solution was made by dissolving commercial salt (sodium chloride) in freshwater at 36 g/L concentration. Freshwater has a density (ρ_f) of 1000 g/L and seawater has a density (ρ_s) of 1025 g/L,

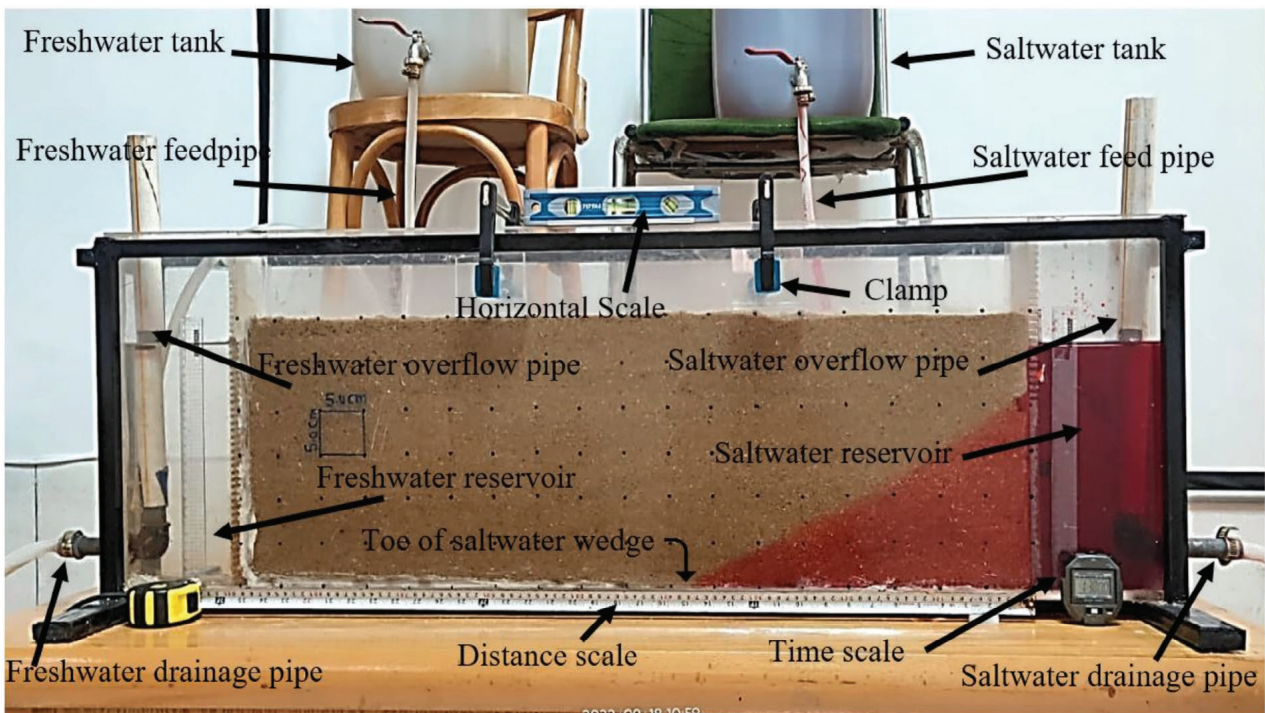


Fig. 1 - Schematic diagram of the experimental setup.

Fig. 1 - Rappresentazione schematica del setup sperimentale.

measured using a densitometer (Alfa Mirage sd-200 L). To discern seawater from the freshwater, the seawater was colored with red coloring with a concentration of 20-gram dye per 40 liters. Two tanks were utilized to deliver saltwater and freshwater at steady flow rates via saltwater and freshwater feed pipelines, respectively. Adjustable drainage pipes were used to manage the freshwater and saltwater levels.

Experimental Procedure

The side reservoirs and the porous medium tank were initially filled with freshwater at the start of each experiment. The saltwater and freshwater reservoir's constant heads were adjusted using drainage pipelines. During the experiments, the estimated head variations were 1.0 mm. The hydraulic gradient (J) between the two heads produced a flow from the freshwater reservoir to the saltwater reservoir. The average hydraulic conductivity (K) of each type of sand was determined using Darcy's law within the experimental sandbox tank, based on the hydraulic gradient and the measured freshwater discharge from the drainage pipe. The hydraulic conductivity was estimated to be equal to 0.337 and 0.7 cm/s for the low K and high K aquifers, respectively. A shut-off wall is fitted to isolate the saltwater reservoir from the central tank once the flow has been measured. In the saltwater reservoir, the colored saltwater was then used to replace the freshwater. By removing the intermediate wall between the aquifer medium and the saltwater reservoir, the SWI process in the aquifer medium was commenced. For scenario 1, the saltwater level on the right side was 26.5 cm. The inland groundwater head on the left increased from 27.7 to 27.9, and then to 28.1 cm. For scenario 2, the inland head on the left-hand side was fixed at 28.1 cm. The saltwater level rose from 26.5 to 26.8, then to 27.1 cm as illustrated in Table 1. A total number of ten experimental cases were conducted that can be divided into two groups: five cases for low K (0.377 cm/s) and five cases for high K (0.7 cm/s).

At the saltwater boundary, freshwater discharge flows upward and floats above the saltwater until draining out. An excess quantity of saltwater solution was continuously fed into the saltwater reservoir to guarantee that any potential freshwater floating on the surface was flushed out. The experiments were conducted after the density measurements had stabilized. Toe position, a commonly used quantitative

metric for characterizing SWI in coastal aquifers (Armanuos et al., 2019; Gao et al., 2021), was measured every 10 minutes until the SWI wedge achieved a steady state.

Numerical Model (SEAWAT)

To simulate groundwater variable-density flow, SEAWAT has been used extensively (Guo & Langevin, 2002). SEAWAT was used in the current study to construct a numerical model of salt transport to assess the effect of SLR on groundwater in coastal aquifers.

Governing Equations

Equations (1) and (2), respectively, depict the flow and transport equations used in the SEAWAT.

$$\frac{\partial}{\partial \alpha} \left(\rho k_{f\alpha} \left[\frac{\partial h_f}{\partial \alpha} + \frac{\rho - \rho_f}{\rho_f} \frac{\partial Z}{\partial \alpha} \right] \right) + \frac{\partial}{\partial \beta} \left(\rho k_{f\beta} \left[\frac{\partial h_f}{\partial \beta} + \frac{\rho - \rho_f}{\rho_f} \frac{\partial Z}{\partial \beta} \right] \right) + \frac{\partial}{\partial \gamma} \left(\rho k_{f\gamma} \left[\frac{\partial h_f}{\partial \gamma} + \frac{\rho - \rho_f}{\rho_f} \frac{\partial Z}{\partial \gamma} \right] \right) = \rho S_f \frac{\partial h_f}{\partial t} + \theta \frac{\partial \rho}{\partial C} \frac{\partial C}{\partial t} - \rho_s q_s \quad 1$$

where α , β , and γ are the direction of groundwater flow; t is the time; $k_{f\alpha}$, $k_{f\beta}$ and $k_{f\gamma}$ are the hydraulic conductivity in the three directions, respectively; θ is the effective porosity; S_f is the specific storage; ρ_f is the freshwater density; ρ is the groundwater density at a point in the aquifer; q_s and ρ_s represent the volume and density of the dissolved material, respectively.

$$\frac{\partial (\theta C^k)}{\partial t} = \nabla (\theta D_{ij} \nabla C^k) - \nabla (\theta V_i C^k) + q_s C_k^S + \sum R_n \quad 2$$

where C^k is the solute substance concentration; $\sum R_n$ is the chemical substance reaction term in the aquifer; D represents the coefficient tensor of hydrodynamic dispersion; V_i is the fluid average linear velocity; C_k^S is the value of the source or sink concentration of species k .

Mesh Discretization

The SEAWAT simulation area consists of a 2-D vertical cross section in dimensions of 90.0 cm · 28.0 cm that is uniformly discretized to a finite-difference mesh of size $\Delta_x \Delta_z = 0.5 \text{ cm} \cdot 0.5 \text{ cm}$, as shown in Figure 2. To ensure

Tab. 1 - Summary of investigated cases for each aquifer.

Tab. 1 - Riepilogo dei casi investigati per ogni acquifero.

Scenario No.	Case No.	Freshwater head (h_f) (cm)	Saltwater head (h_s) (cm)	Hydraulic gradient (J) (-)	Hydraulic conductivity (K)
base	1	27.7	26.5	0.0133	5 cases for low K (0.377 cm/s) and 5 cases for high K (0.7 cm/s)
1	2	27.9	26.5	0.0156	
	3	28.1	26.5	0.0178	
2	4	28.1	26.8	0.0144	
	5	28.1	26.7	0.0111	
Total					10 cases

numerical stability, the grid spacing and dispersivity must satisfy the criterion of Péclet number (Voss & Souza, 1987). The Péclet number ($Pe_m \approx \Delta x / \alpha_l$) is a dimensionless number that quantifies the proportion of local advective transport to local diffusion and dispersive transport, where α_l is the longitudinal dispersivity of the porous media. Porous media was given a longitudinal dispersivity (α_l) of 0.15 cm, a value commonly used in laboratory experiments (Sun et al., 2019; Chang et al., 2019; Gao et al., 2021). In this study, the dispersivity value and the grid spatial discretization satisfy the Péclet number criterion ($Pe_m = 3.33 < 4.0$), and thus provide sufficient numerical stability.

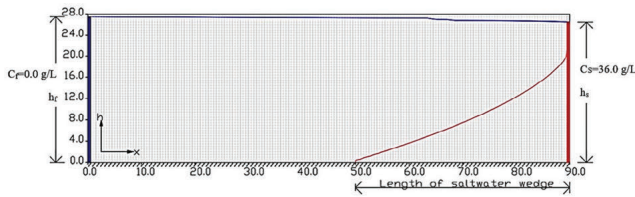


Fig. 2 - Boundary conditions and grid spacing for the numerical modeling.

Fig. 2 - Condizioni al contorno e dimensione della griglia per il modello numerico.

Boundary Conditions

The salt concentration (C_s) was set to 36 g/L at the boundary on the right side with a constant head (h_s) of 26.5 cm. The salt concentration of freshwater on the left side was fixed at $C_f = 0.0$ g/L. Freshwater and saltwater densities were 1000 g/L and 1025 g/L, respectively. Figure 2 represents the boundary conditions of the numerical simulations.

Tab. 2 - Summary of model parameters.

Tab. 2 - Riepilogo dei parametri del modello.

Parameter	Value	Unit
Domain length (L)	90	cm
Domain height (H)	28	cm
Freshwater head (h_f)	27.7, 27.9, 28.1	cm
Saltwater head (h_s)	26.5, 26.8, 27.1	cm
Freshwater density (ρ_f)	1000	g/L
Saltwater density (ρ_s)	1025	g/L
Freshwater concentration (C_f)	0.0	g/L
Saltwater concentration (C_s)	36.0	g/L
Hydraulic conductivity (K_H) High K aquifer	0.7	cm/s
Hydraulic conductivity (K_L) Low K aquifer	0.377	cm/s
Porosity (n)	0.4	-
Longitudinal dispersivity (α_L)	0.15	cm
Transversal dispersivity (α_T)	0.015	cm
Specific yield (S_y)	0.2	-

Steady State Analytical Equations

During the experiments, for the studied aquifers, the saltwater-freshwater interface reached five steady-state conditions. We compared the steady-state saltwater wedges with the analytical solutions developed by Ghyben (1888), Glover (1959), Rumer Jr & Harleman (1963), Verruijt (1968), and Kashef (1983). For all the investigated cases, the average significant correlation coefficient matrices were constructed to assess the match between the experimental, the analytical, and the numerical results. To identify the suitable analytical equation, the maximum and average difference matrices were calculated for all the cases under consideration.

Ghyben (1888) derived an analytical equation for the sharp interface position, and Herzberg (1901) independently reached the same expression. Their equation connects the elevation of the saltwater-freshwater interface to the elevation of the water table in an unconfined aquifer

$$z = \frac{\rho_f}{\rho_s - \rho_f} h_f \tag{3}$$

Where, ρ_s is the saltwater density, ρ_f is the freshwater density, z is the depth of a point on the interface below sea level, and h_f is the elevation of the water table above sea level at that point.

Glover (1959) derived an expression for describing SWI sharp interface in a coastal aquifer while allowing for freshwater seaward flow. His expression could be used to calculate the interface position:

$$z^2 = \frac{2\rho_f qx}{\Delta\rho K} + \left(\frac{\rho_f q}{\Delta\rho K} \right)^2 \tag{4}$$

Where q is the freshwater discharge rate; K is the aquifer hydraulic conductivity, ρ_f is the freshwater density, $\Delta\rho = \rho_s - \rho_f$, x is the distance from the shoreline, and z is the depth of the sharp interface below the sea level.

Rumer Jr & Harleman (1963) analysis of the parabolic interface is based on Glover (1959) expression.

$$z^2 = \frac{2\rho_f qx}{\Delta\rho K} + 0.55 \left(\frac{\rho_f q}{\Delta\rho K} \right)^2 \tag{5}$$

Where q is the freshwater discharge rate; K is the aquifer hydraulic conductivity, ρ_f is the freshwater density, $\Delta\rho = \rho_s - \rho_f$, x is the distance from the shoreline, and z is the depth of the sharp interface below the sea level.

Verruijt (1968) demonstrated that the interface are parabolas represented by:

$$z = - \left[\left(\frac{q}{\beta K} \right)^2 \cdot \left(\frac{1-\beta}{1+\beta} \right) + 2 \left(\frac{q}{\beta K} \right) \cdot \left(\frac{x}{1+\beta} \right) \right]^{1/2} \tag{6}$$

Where x is the distance from the seashore, z is the depth of the sharp interface below the sea level (positive upwards), q is the seaward freshwater discharge, and $\beta = (\rho_s - \rho_f) / \rho_f$.

According to Kashef (1983), the actual saltwater interface is underneath the Ghyben-Herzberg interface and can be calculated for the vertical outflow interface as follows:

$$D_{x_{dv}}/h_o \cong \left[\left(\frac{D_{xu}}{\alpha h_o} \right) + 0.1375 \left(\frac{1-x}{m^2} \right) \right]^{1/2} \quad 7$$

$$D_{xu} = D_{xd} \cdot \alpha \quad 8$$

$$\alpha = \frac{\rho_s - \rho_f}{\rho_f} \quad 9$$

$$D_{xd} = \frac{2qx}{\alpha K} \quad 10$$

$$m = \frac{L}{h_o} \quad 11$$

Where $D_{x_{dv}}$ is the depth of the interface corresponding to vertical outflow surface, L is the SWI wedge length measured inland from the shoreline, h_o is the depth of the underlying impervious layer below the sea level in the unconfined aquifer, x is the distance from the shoreline, D_{xu} is the height of the groundwater table above sea level, K is the aquifer hydraulic conductivity, and q is the freshwater flow into the sea.

Finally, the steady-state experimental saltwater toe lengths were compared with the analytical solutions developed by Lu et al. (2015) and Anderson (2021). Lu et al. (2015) derived an equation to calculate the locations of SWI interface toe in unconfined coastal aquifers:

$$X_{toe} = \frac{L(1+\beta)H_s^2}{H_f^2\beta^2 - (1+\beta)\beta H_s^2} \quad 12$$

$$\beta = \frac{\rho_f}{\rho_s - \rho_f} \quad 13$$

Where X_{toe} is the saltwater toe length, β is the density ratio, H_s is the mean sea level above the bottom of the aquifer, ρ_f is the freshwater density, ρ_s is the density of the seawater, and H_f is the freshwater head at a distance L from the saltwater boundary.

Anderson (2021) derived a new analytical solution for toe length in unconfined aquifers. The two-term approximation is expressed as:

$$X_{toe} \approx \left(1 + \frac{K^*}{K} \right) \frac{k^* H_s}{2Q_o} - \left(\frac{2}{3} - \frac{K^*}{K} \right) \frac{Q_o}{2K^* H_s} \quad 14$$

$$k^* = K \left(\frac{\rho_s - \rho_f}{\rho_f} \right)$$

Where X_{toe} is the toe length, H_s is the sea level above the bottom of the aquifer, Q_o is seaward groundwater discharges, K is the aquifer hydraulic conductivity, ρ_f is the freshwater density, and ρ_s is the density of the seawater.

Results and discussions

This section presents a summary of the data obtained from the SWI experiments and numerical simulations. Both steady-state and transient data sets are used. The transient analysis consisted in comparing the transient numerical groundwater levels and salt concentrations to those observed in the laboratory experiments under the receding-front condition and advancing front condition. The temporal toe penetration and area of the seawater wedge were then calculated for the two scenarios 1 and 2. The steady-state analysis compared the steady-state saltwater wedges to the analytical solutions developed by Ghyben (1888), Glover (1959), Rumer Jr & Harleman (1963), Verruijt (1968), and Kashef (1983). The 50% seawater salinity isoline was identified in the model by visualizing the 18.0 g/L contour line. While in the experiment, the 50% isoline was identified by monitoring the saltwater wedge shape (Gao et al., 2021).

Transient Analyses

The toe penetration length values obtained by the numerical model were comparable to the experimental toe penetration length for all cases in the low K aquifer (Fig. 3) presenting a maximum Root Mean Square Error (RMSE) equal to 0.33 cm and an average significant correlation coefficient (R^2) greater than 0.9817. Similarly, in the high K aquifer (Fig. 4), the maximum RMSE is equal to 0.92 cm and the average significant correlation coefficient (R^2) is greater than 0.9335, as illustrated in Table 3. The numerical model, which has been successfully benchmarked against a vast amount of comprehensive experimental data, can be dependably used to further explore the impact of variable-head inland boundary conditions and SLR on saltwater intrusion characteristics.

Steady State Analyses

Figure 5 shows the steady state SWI experimental results for the low K aquifer (a) and the high K aquifer (b). The experiment saltwater penetration length and the area of saltwater wedges at the steady-state conditions for the two investigated unconfined aquifers are summarized in Table 4. The steady-state saltwater wedge locations (50% isoline) predicted by SEAWAT were compared with the experimental results. The results show a good match between the model and the experimental records. In the high K aquifer cases, the SEAWAT simulations showed some minor differences.

Tab. 3 - Comparison of transient numerical and experimental SWI toe length.

Tab. 3 - Confronto tra risultati numerici in condizioni transitorie e risultati sperimentali ottenuti relativamente alla distanza alla quale l'interfaccia acqua dolce-acqua salata interseca il fondo impermeabile dell'acquifero (toe length).

Scenario No.	Case No.	Freshwater head (h_f) (cm)	Saltwater head (h_s) (cm)	Hydraulic gradient (J) (-)	Root Mean Square Error (RMSE) (cm)		The average significant correlation coefficient (R^2)	
					Low K	High K	Low K	High K
base	1	27.7	26.5	0.0133	0.33	0.76	0.9987	0.9962
1	2	27.9	26.5	0.0156	0.21	0.92	0.9905	0.9335
	3	28.1	26.5	0.0178	0.25	0.43	0.9817	0.9700
2	4	28.1	26.8	0.0144	0.12	0.33	0.9981	0.9965
	5	28.1	27.1	0.0111	0.27	0.41	0.9959	0.9962
Maximum					0.33	0.92		
Minimum							0.9817	0.9335

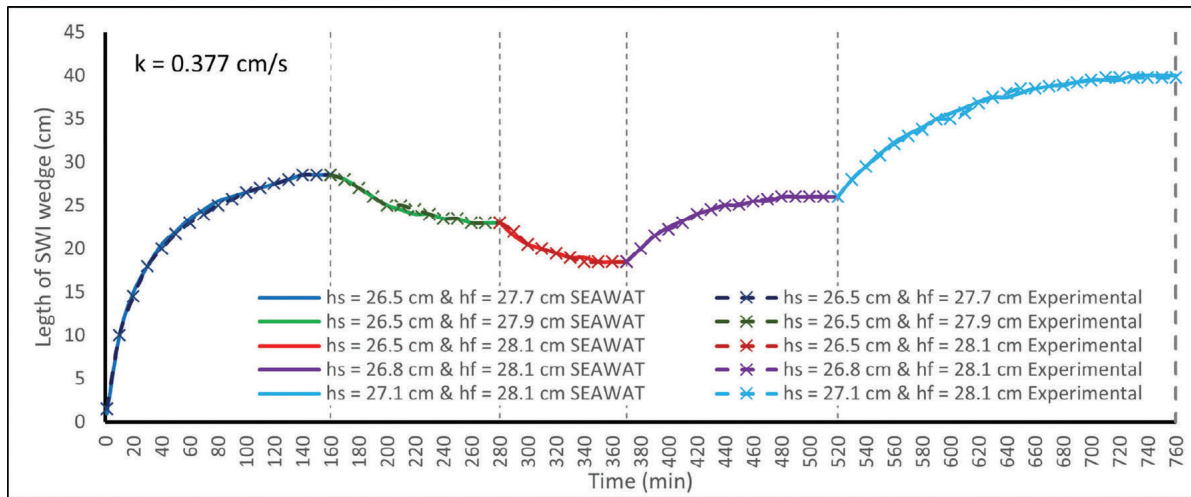


Fig. 3 - Transient numerical and experimental saltwater wedge length for low K aquifer ($K = 0.377$ cm/s).

Fig. 3 - Confronto tra risultati numerici in condizioni transitorie e risultati sperimentali ottenuti relativamente all'ampiezza del cuneo di intrusione salina per l'acquifero a bassa permeabilità ($K = 0.377$ cm/s).

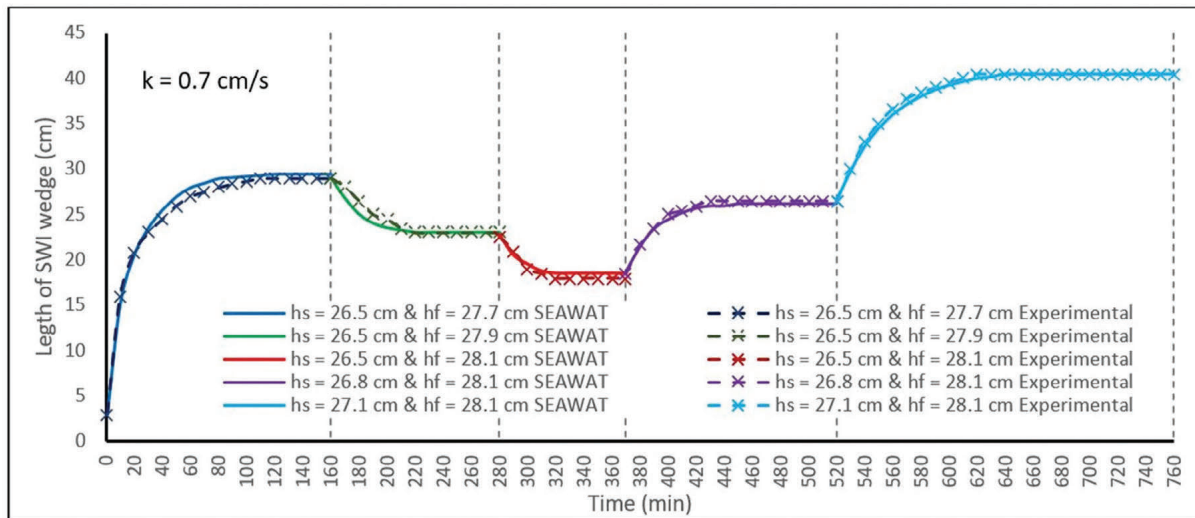


Fig. 4 - Transient numerical and experimental saltwater wedge length for high K aquifer ($K = 0.7$ cm/s).

Fig. 3 - Confronto tra risultati numerici in condizioni transitorie e risultati sperimentali ottenuti relativamente all'ampiezza del cuneo di intrusione salina per l'acquifero ad alta permeabilità ($K = 0.7$ cm/s).

Tab. 4 - The length and area of the steady-state seawater wedge in each experiment group.

Tab. 4 - Ampiezza e area del cuneo di intrusione salina in condizioni stazionarie per ogni caso sperimentale.

Scenario No.	Case No.	Freshwater head (h_f) (cm)	Saltwater head (h_s) (cm)	Hydraulic gradient (J) (-)	Toe Penetration of Saltwater Wedge (cm)		Area of Seawater Wedge (cm ²)		Time to reach steady state (min)	
					Low K	High K	Low K	High K	Low K	High K
base	1	27.7	26.5	0.0133	28.5	29.5	229	237	140	110
1	2	27.9	26.5	0.0156	23.0	23	177	175	100	60
	3	28.1	26.5	0.0178	18.5	18	132	132	90	40
2	4	28.1	26.8	0.0144	26.0	26.5	204	208	110	80
	5	28.1	27.1	0.0111	40.0	40.5	346	349	210	120



Fig. 5 - Experimental steady-state saltwater wedges for the low K (a) and the high K (b) aquifers.

Fig. 5 - Cuneo di intrusione salina in condizioni stazionarie per gli acquiferi a bassa permeabilità (a) e ad alta permeabilità (b).

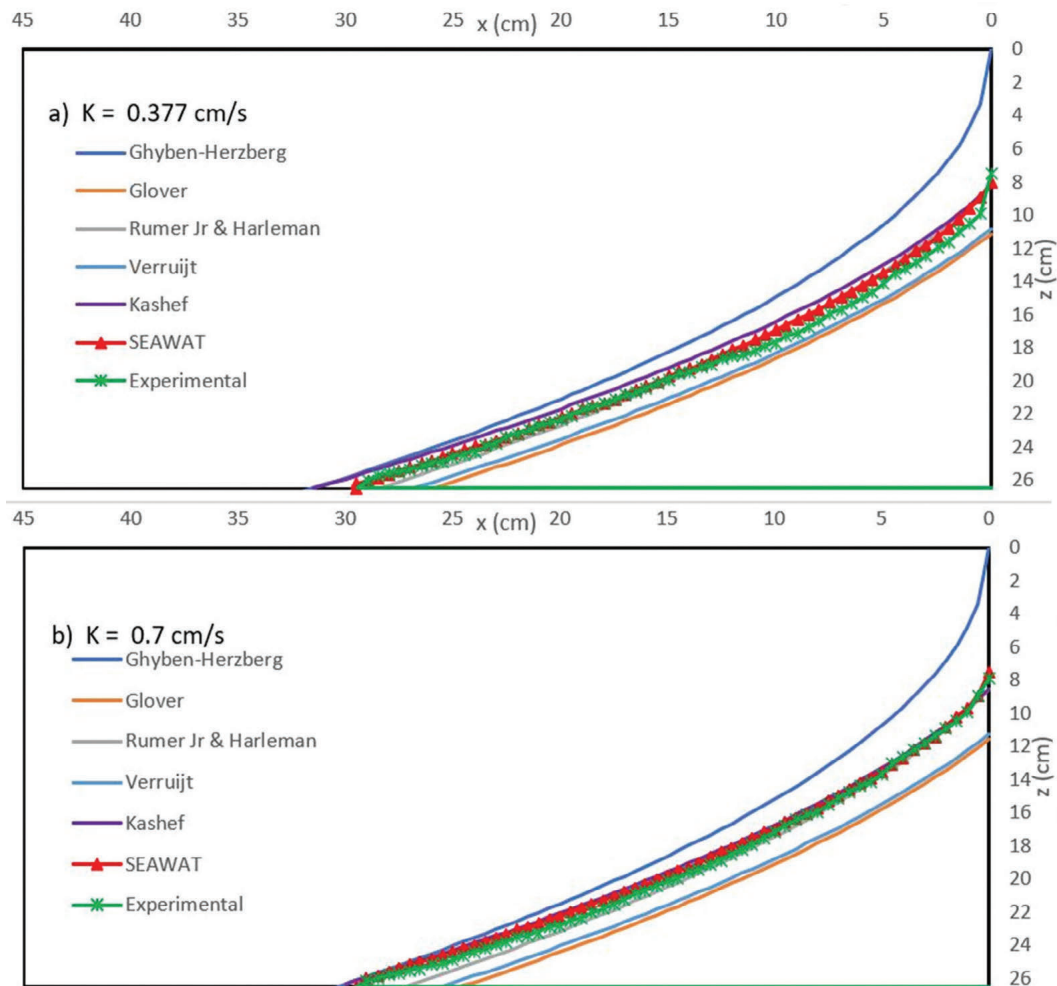
Case 1 ($h_f = 27.7$ cm and $h_s = 26.5$ cm)

Fig. 6 - Steady-state saltwater wedge profiles at $h_f = 27.7$ cm and $h_s = 26.5$ cm in low K (a) and high K (b) aquifers.

Fig. 6 - Profili del cuneo di intrusione salina in condizioni stazionarie con $h_f = 27.7$ cm e $h_s = 26.5$ cm per gli acquiferi a bassa permeabilità (a) e ad alta permeabilità (b).

The initial condition in our study was the first steady state condition, or SS1, shown in Figure 6. For this condition, freshwater and saltwater heads of 27.7 cm and 26.5 cm, respectively, were used. According to the analysis of the experimental data, the toe of the wedge was roughly located 29.5 cm from the saltwater boundary for the two aquifers. At SS1, the elevation of the saltwater interface was 19 cm and 18.6 cm at the saltwater boundary for the low K and high K aquifers, respectively. The freshwater discharge through the aquifer was estimated by measuring the overflow at both sides of the sandbox. The net freshwater flow that was calculated using these data was $0.84 \text{ cm}^3/\text{s}$ and $1.85 \text{ cm}^3/\text{s}$ for the low K and high K aquifers, respectively.

For the low K aquifer, the penetration length of saltwater intrusion was estimated by Ghyben (1888), Glover (1959), Rumer Jr & Harleman (1963), Verruijt (1968), and Kashef (1983) to be equal to 31.5, 25.5, 28.0, 26.5, and 31.5 cm, respectively. The resulting saltwater wedges from the analytical equation were compared to the experimental data.

The RMSE is equal to 2.68, 1.52, 0.60, 1.19, and 0.88 cm, respectively, and the average significant correlation coefficient (R^2) is equal to 0.9978, 0.9971, 0.9982, 0.9972, and 0.9981, respectively. The maximum R^2 value (0.9982) and the minimum RMSE value (0.60 cm) were obtained by Rumer Jr & Harleman's equation.

For the high K aquifer, the penetration length of saltwater intrusion was estimated using the same equations as for the low K aquifer. These estimates were found to be equal to 30.0, 24.5, 27.0, 25.0, and 30.0 cm, respectively. The resulting saltwater wedges from the analytical equation were compared to the experimental records. The RMSE is equal to 2.36, 2.02, 0.51, 1.69, and 0.49 cm, respectively, and the average significant correlation coefficient (R^2) is equal to 0.9965, 0.9984, 0.9994, 0.9985, and 0.9993, respectively. The maximum R^2 value (0.9994) was obtained by Rumer Jr & Harleman's equation and the minimum RMSE value (0.49 cm) was obtained by Kashef's equation.

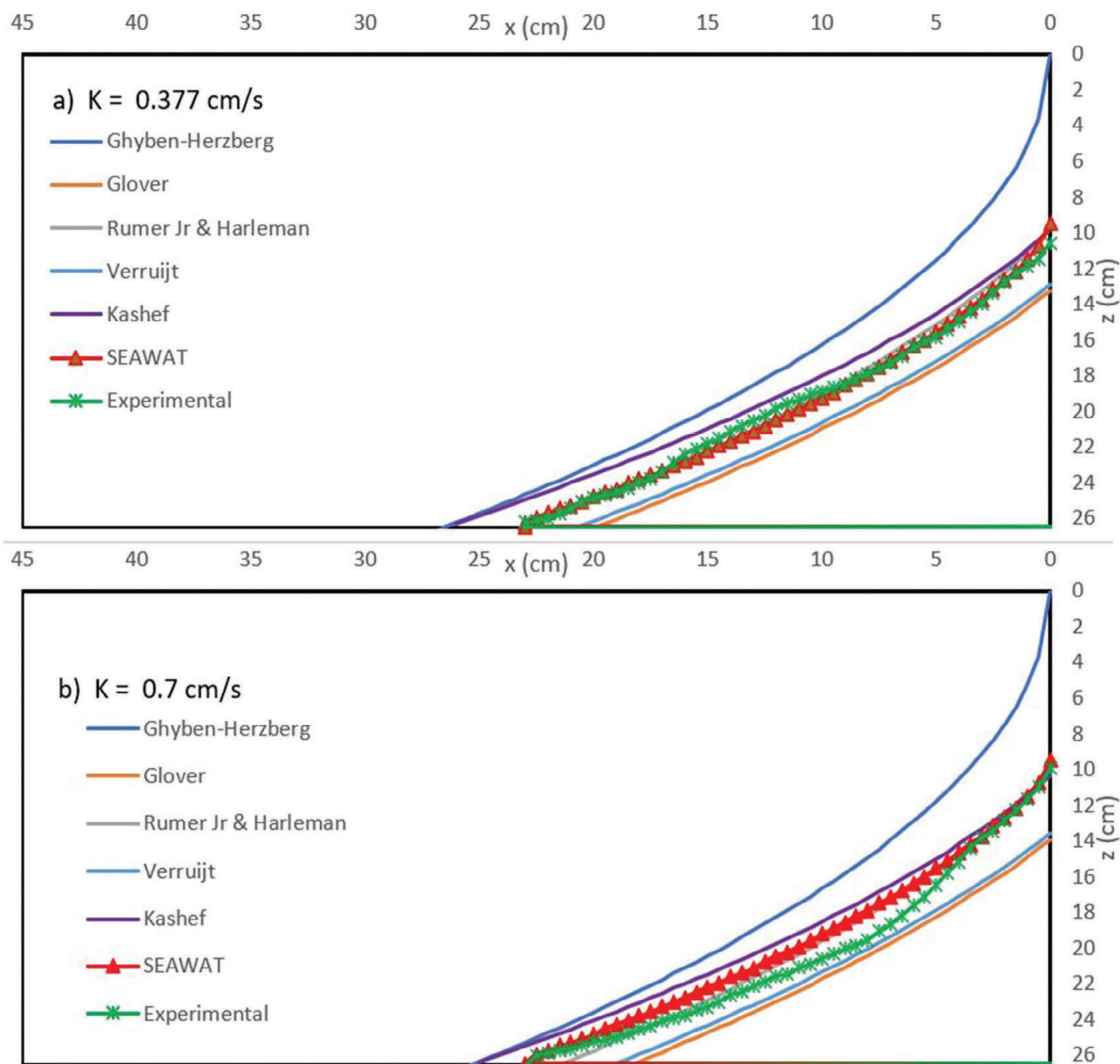
Case 2 ($h_f=27.9$ cm and $h_s = 26.5$ cm)

Fig. 7 - Steady-state saltwater wedge profiles at $h_f = 27.9$ cm and $h_s = 26.5$ cm in low K (a) and high K (b) aquifers.

Fig. 7 - Profili del cuneo di intrusione salina in condizioni stazionarie con $h_f = 27.9$ cm e $h_s = 26.5$ cm per gli acquiferi a bassa permeabilità (a) e ad alta permeabilità (b).

To begin the salt-wedge receding condition, the freshwater head was abruptly increased from 27.7 to 27.9 cm. As the wedge drifted from the SS1 to the second steady state condition SS2, the transient data were continuously collected. The system reached SS2 in about 100 min and 60 min for the low K and high K aquifers, respectively. The saltwater wedge toe, according to the analysis of the steady-state data, was roughly located 23 cm away from the saltwater boundary, shown in Figure 7. The elevation of the saltwater interface at the saltwater boundary was 16 cm and 16.6 cm for the low K and high K aquifers, respectively. The freshwater discharge that was flowing through the aquifers was calculated to be $1.0 \text{ cm}^3/\text{s}$ and $2.23 \text{ cm}^3/\text{s}$ for the low K and high K aquifers, respectively.

The penetration length of saltwater intrusion was calculated for the low K aquifer using the equations of Ghyben (1888), Glover (1959), Rumer Jr & Harleman (1963), Verruijt (1968), and Kashef (1983) to be 26.0, 19.5, 22.5, 20.5, and 26.0 cm, respectively. The resulting saltwater wedges from the

analytical equation were compared to the outcomes of the experiments. The average significant correlation coefficients (R^2) were 0.9909, 0.9975, 0.9978, 0.9976, and 0.9978, respectively, and the root mean square errors (RMSE) were equal to 3.50, 2.02, 0.55, 1.65, and 1.11 cm, respectively. Rumer Jr & Harleman's equation produced the highest R^2 value of 0.9978 and the lowest RMSE value of 0.55 cm.

The penetration length of saltwater intrusion was calculated for the high K aquifer using the same equations as for the low K aquifer. These estimates were found to be equal to 25.0, 18.0, 21.0, 19.0, and 25.0 cm, respectively. The resulted saltwater wedges from the analytical equation were compared to the outcomes of the experiments. The average significant correlation coefficients (R^2) were 0.9951, 0.9869, 0.9906, 0.9871, and 0.9897, respectively, and the root mean square errors (RMSE) were equal to 2.86, 2.11, 0.80, 1.75, and 1.51 cm, respectively. Rumer Jr & Harleman's equation produced the highest R^2 value of 0.9951 and the lowest RMSE value of 0.80 cm.

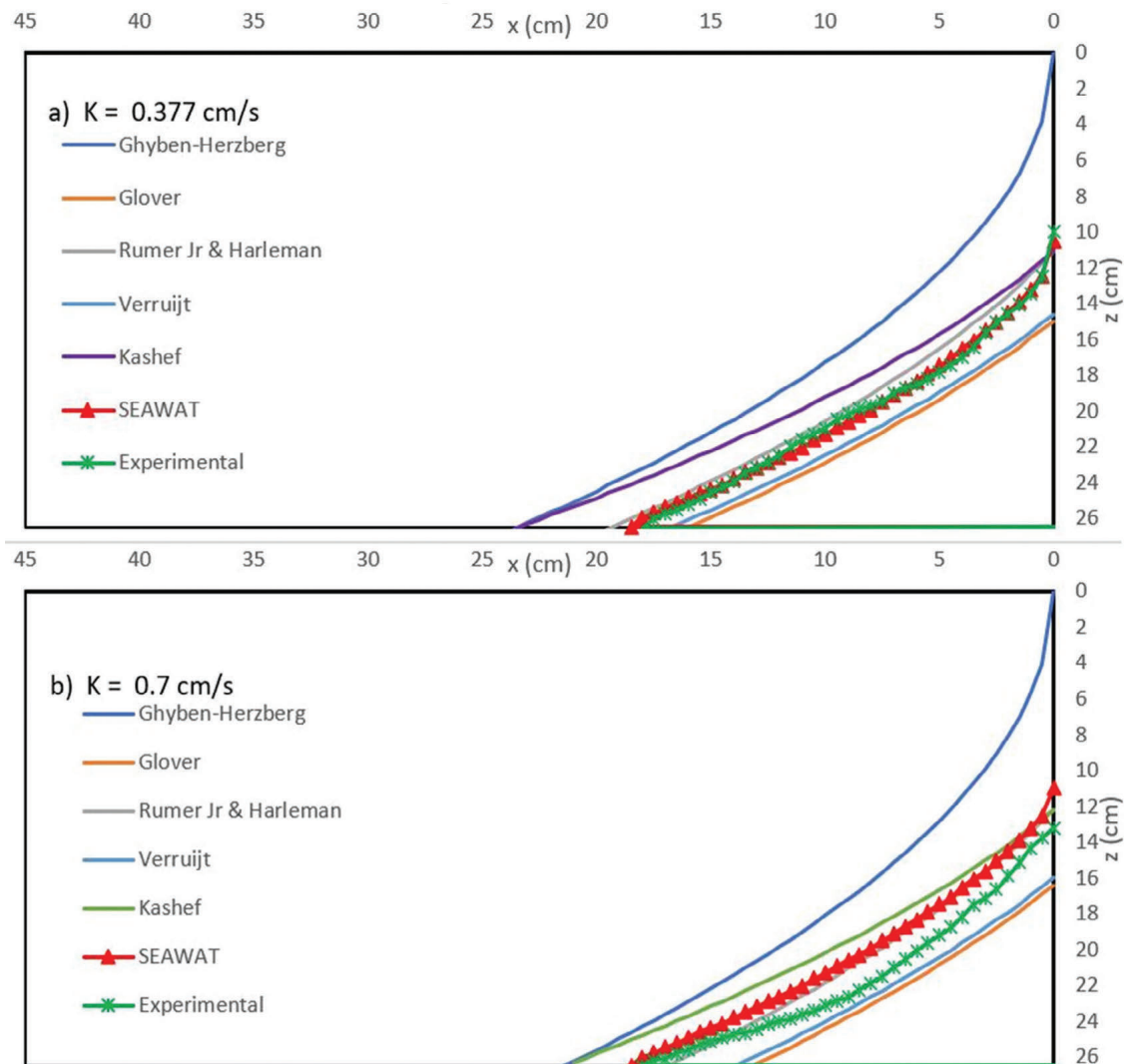
Case 3 ($h_f = 28.1$ cm and $h_s = 26.5$ cm)

Fig. 8 - Steady-state saltwater wedge profiles at $h_f = 28.1$ cm and $h_s = 26.5$ cm in low K (a) and high K (b) aquifers.

Fig. 8 - Profili del cuneo di intrusione salina in condizioni stazionarie con $h_f = 28.1$ cm e $h_s = 26.5$ cm per gli acquiferi a bassa permeabilità (a) e ad alta permeabilità (b).

To continue the salt-wedge receding condition, the freshwater head was abruptly increased from 27.9 to 28.1 cm. The system reached the third steady state SS3 in about 90 min and 40 min for the low K and high K aquifers, respectively. According to the analysis of the steady-state data, the saltwater wedge toe was roughly 18 cm away from the saltwater boundary, as shown in Figure 8. The elevation of the saltwater interface at the saltwater boundary was 16.5 cm and 13.5 cm for the low K and high K aquifers, respectively. The net freshwater discharge that was flowing through the aquifers was calculated to be $1.13 \text{ cm}^3/\text{s}$ and $2.63 \text{ cm}^3/\text{s}$ for the low K and high K aquifers, respectively.

For the low K aquifer, the penetration length of saltwater intrusion was estimated by Ghyben (1888), Glover (1959), Rumer Jr & Harleman (1963), Verruijt (1968), and Kashef (1983) to be equal to 23.0, 15.5, 19.0, 16.5, and 23.5 cm, respectively. The resulting saltwater wedges from the analytical equation were compared to the experimental data.

The RMSE is equal to 4.50, 2.18, 1.25, 1.80, and 1.85 cm, respectively, and the average significant correlation coefficient (R^2) is equal to 0.9936, 0.9850, 0.9881, 0.9852, and 0.9872, respectively. The maximum R^2 value (0.9936) was obtained by Ghyben's equation and the minimum RMSE value (0.96 cm) was obtained by Rumer Jr & Harleman's equation.

For the high K aquifer, the penetration length of saltwater intrusion was estimated using the same equations as for the low K aquifer. These estimates were found to be equal to 21.0, 13.0, 16.5, 13.5, and 21.0 cm, respectively. The resulting saltwater wedges from the analytical equation were compared to the experimental records. The RMSE is equal to 5.45, 2.43, 1.25, 2.02, and 2.20 cm, respectively, and the average significant correlation coefficient (R^2) is equal to 0.131, 0.8685, 0.8804, 0.8691, and 0.9827, respectively. The maximum R^2 value (0.9827) was obtained by Kashef's equation and the minimum RMSE value (1.25 cm) was obtained by Rumer Jr & Harleman's equation.

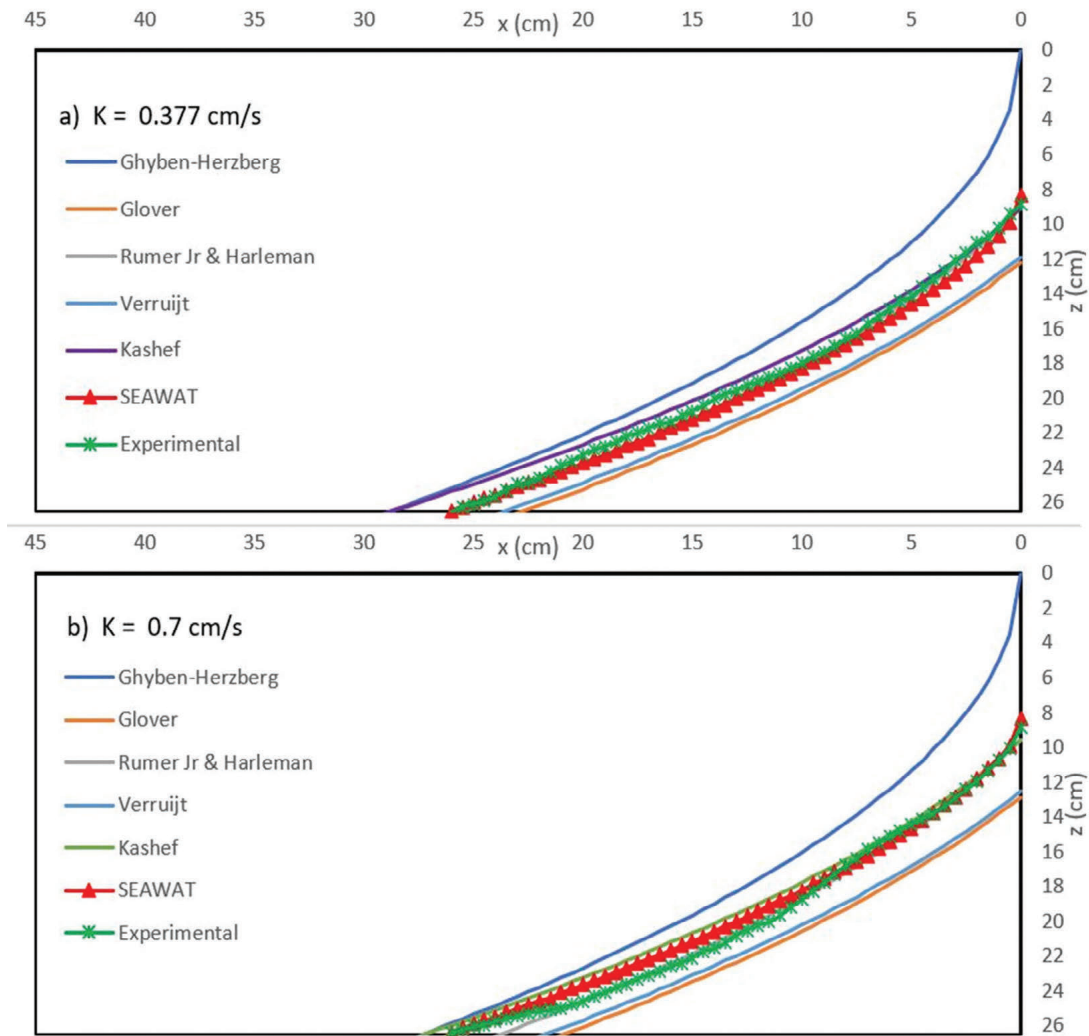
Case 4 ($h_f = 28.1$ cm and $h_s = 26.8$ cm)

Fig. 9 - Steady-state saltwater wedge profiles at $h_f = 28.1$ cm and $h_s = 26.8$ cm in low K (a) and high K (b) aquifers.

Fig. 9 - Profili del cuneo di intrusione salina in condizioni stazionarie con $h_f = 28.1$ cm e $h_s = 26.8$ cm per gli acquiferi a bassa permeabilità (a) e ad alta permeabilità (b).

The saltwater head was instantly increased from 26.5 to 26.8 cm to start transient SWI under SLR conditions. The transient data were collected at periodic intervals as the wedge advanced from SS3 to SS4. The system reached the fourth steady state SS4 in about 110 min and 80 min for the low K and high K aquifers, respectively. The toe of the salt wedge, according to the analysis of the steady-state data, was approximately 26 cm and 26.5 cm for the low K and high K aquifers, respectively, away from the saltwater boundary.

The elevation of the saltwater interface at the saltwater boundary was equal to 17.9 cm for both the low K and high K aquifers, as shown in Figure 9. The net freshwater discharge that was flowing through the aquifers was estimated to be 0.92 cm³/s and 2.06 cm³/s for the low K and high K aquifers, respectively.

The penetration length of saltwater intrusion was calculated for the low K aquifer using the equations of Ghyben (1888), Glover (1959), Rumer Jr & Harleman (1963), Verruijt (1968), and Kashef (1983) to be 29.0, 23.0, 26.0, 24.0, and 29.0

cm, respectively. The resulting saltwater wedges from the analytical equation were compared to the outcomes of the experiments. The average significant correlation coefficients (R^2) were 0.9941, 0.9986, 0.9992, 0.9986, and 0.9991, respectively, and the root mean square errors (RMSE) were equal to 2.60, 2.10, 0.43, 1.76, and 0.67 cm, respectively. Rumer Jr & Harleman's equation produced the highest R^2 value (0.9992) and the lowest RMSE value (0.43 cm).

The penetration length of saltwater intrusion was calculated for the high K aquifer using the same equations as for the low K aquifer. These estimates were found to be equal to 27.5, 21.0, 24.0, 22.0, and 27.5 cm, respectively. The resulting saltwater wedges from the analytical equation were compared to the outcomes of the experiments. The average significant correlation coefficients (R^2) were 0.9939, 0.9950, 0.9965, 0.9951, and 0.9963, respectively, and the root mean square errors (RMSE) were equal to 2.96, 2.20, 0.52, 1.85, and 0.93 cm, respectively. Rumer Jr & Harleman's equation produced the highest R^2 value (0.9965) and the lowest RMSE value (0.52 cm).

Case 5 ($h_f = 28.1$ cm and $h_s = 27.1$ cm)

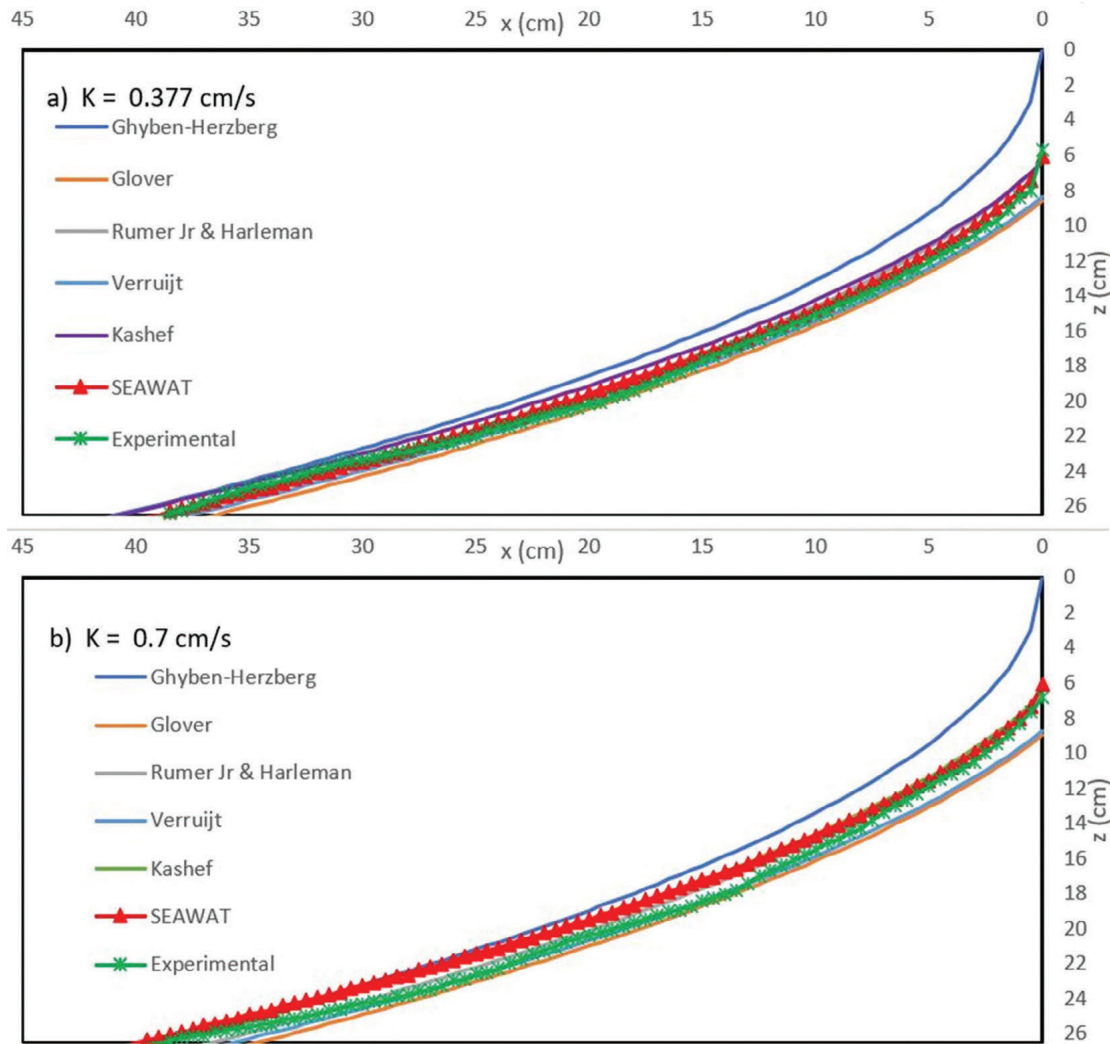


Fig. 10 - Steady-state saltwater wedge profiles at $h_f = 28.1$ cm and $h_s = 27.1$ cm in low K (a) and high K (b) aquifers.

Fig. 10 - Profili del cuneo di intrusione salina in condizioni stazionarie con $h_f = 28.1$ cm e $h_s = 27.1$ cm per gli acquiferi a bassa permeabilità (a) e ad alta permeabilità (b).

The saltwater head was abruptly increased from 26.8 to 27.1 cm to continue the salt-wedge advancing condition. The system reached the fifth steady state SS in about 210 min and 120 min for the low k and high K aquifers, respectively. The saltwater wedge toe, according to the analysis of the steady-state data, was roughly 40 cm and 40.5 cm for the low K and high K aquifers, respectively, away from the saltwater boundary, as shown in Figure 10. The elevation of the saltwater interface at the saltwater boundary was equal to 21.4 cm and 20.23 cm for the low K and high K aquifers, respectively. The net freshwater flux that was flowing through the aquifers was estimated to be 0.65 cm³/s and 1.44 cm³/s for the low K and high K aquifers, respectively.

For the low K aquifer, the penetration length of saltwater intrusion was estimated by Ghyben (1888), Glover (1959), Rumer Jr & Harleman (1963), Verruijt (1968), and Kashef (1983) to be equal to 42.5, 38.0, 40.0, 39.0, and 42.5 cm, respectively. The resulting saltwater wedges from the analytical equation were compared to the experimental data.

The RMSE is equal to 1.92, 0.78, 0.52, 0.53, and 0.79 cm, respectively, and the average significant correlation coefficient (R^2) is equal to 0.9986, 0.9980, 0.9988, 0.9980, and 0.9988, respectively. The maximum R^2 value (0.9988) and the minimum RMSE value (0.52 cm) were obtained by Rumer Jr & Harleman's equation.

For the high K aquifer, the penetration length of saltwater intrusion was estimated using the same equations as for the low K aquifer. These estimates were found to be equal to 40.5, 36.0, 38.0, 37.0, and 40.5 cm, respectively. The resulting saltwater wedges from the analytical equation were compared to the experimental records. The RMSE is equal to 2.00, 0.89, 0.49, 0.64, and 0.83 cm, respectively, and the average significant correlation coefficient (R^2) is equal to 0.9976, 0.9971, 0.9983, 0.9971, and 0.9982, respectively. The maximum R^2 value (0.9983) and the minimum RMSE value (0.49 cm) were obtained by Rumer Jr & Harleman's equation.

The statistical analysis of the analytical solution developed by Ghyben (1888), Glover (1959), Rumer Jr & Harleman

(1963), Verruijt (1968), and Kashef (1983), when compared with the numerical and experimental solution, revealed that in most of the investigated cases, Rumer Jr & Harleman's equation was the most suitable choice with a minimal root mean square error (RMSE) and high average significant correlation coefficient (R^2) in the calculated saltwater wedge length (Appendix A).

Comparison between experimental and analytical steady-state saltwater toe length

A comparison between experimental steady-state saltwater toe length and the analytical solutions derived by Lu et al. (2015) and Anderson (2021) for the low K and high K aquifers are presented in Figure 11a and Figure 11b, respectively.

From Figure 11 one can conclude that Lu et al. (2015) equation overestimates the saltwater toe length by about 19.9% and 19% higher than the experimental saltwater toe length with a root mean square error RMSE equal to 5.21 and 5.0 cm for low and high K aquifers, respectively. On the other hand, Anderson's (2021) equation almost fits the measured experimental saltwater toe length with a root mean square error RMSE equal to 0.53 cm for low aquifer and underestimates the saltwater toe length by about 6.7% less than the experimental saltwater toe length with a root mean square error RMSE equal to 1.77 cm for high K aquifers.

CONCLUSIONS

Sea level rise in coastal areas increases saline water intrusion and groundwater contamination. In the current study, we offer a collection of new benchmark data sets for evaluating SWI models taking into account the movement of saltwater in both

transient and steady-state conditions. Several experimental data sets, including transient saltwater wedge data sets as well as steady-state saltwater wedge data sets, were presented. We were able to simulate these data sets successfully using the SEAWAT saltwater intrusion model.

The impact of SLR on groundwater salinity in unconfined aquifers was examined in this study based on both transient and steady-state conditions. Two sets of laboratory tests were conducted, considering scenarios 1 and 2, where the inland head increased from 27.7 to 27.9 to 28.1 cm and the sea level rose from 26.5 to 26.8 to 27.1 cm, respectively. Two different aquifer characteristics were investigated including low conductivity aquifer ($K = 0.377$ cm/s) and high conductivity aquifer ($K = 0.7$ cm/s). In the two homogeneous aquifers, groundwater flow and seawater intrusion were observed during the experiments.

The transient saltwater penetration length increased or decreased rapidly at first, and then tended to stabilize until it reached the steady state for each case. Overall, the saltwater density, dispersivity, and hydraulic conductivity estimations were acceptable. The findings may shed light on how coastal unconfined aquifers are affected by seawater intrusion due to SLR and inland groundwater head.

When compared to transient laboratory experiments, the numerical values of groundwater heads and salinity concentrations agreed well with the experimental data. In the low K aquifer, the RMSE equals 0.33 cm and the average significant correlation coefficient (R^2) is greater than 0.9817. Similarly, in the high K aquifer, the RMSE equals 0.92 cm and the average significant correlation coefficient (R^2) is greater than 0.9335.

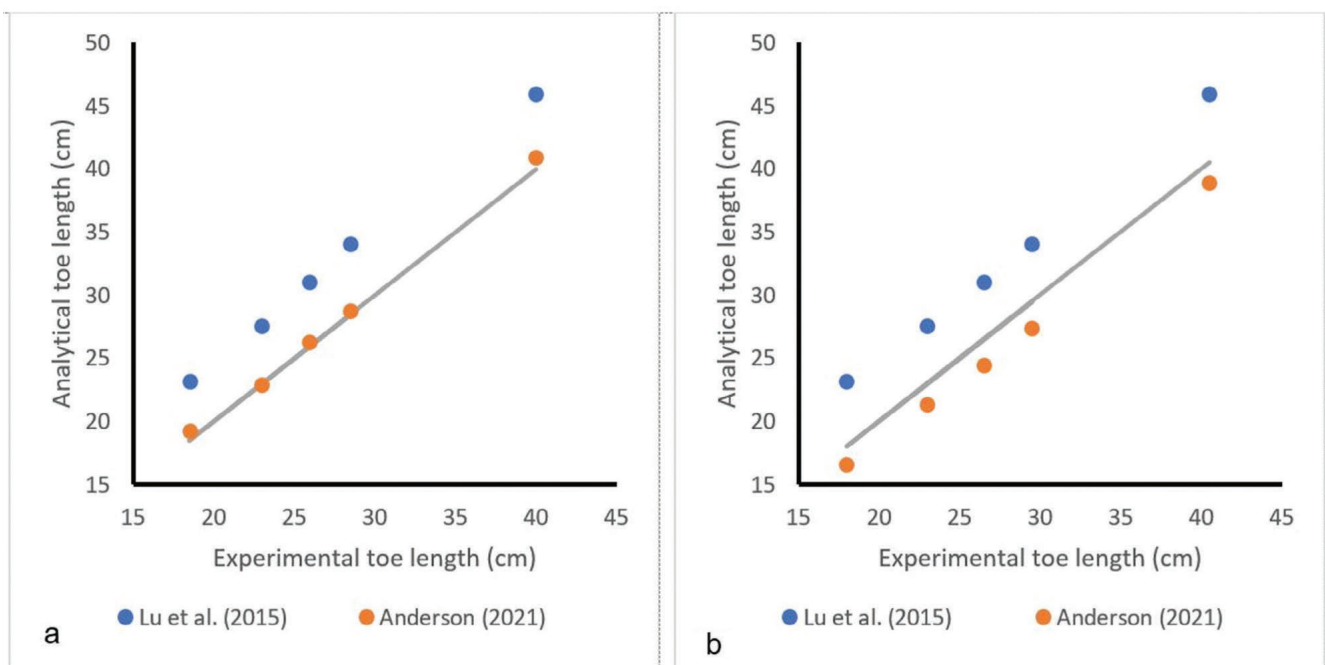


Fig. 11 - Comparison between experimental and analytical steady-state saltwater toe length for the low K (a) and high K (b) aquifers.

Fig. 11 - Confronto tra risultati sperimentali e i risultati analitici in condizioni stazionarie relativamente alla distanza alla quale l'interfaccia acqua dolce-acqua salata interseca il fondo impermeabile dell'acquifero (toe length) per gli acquiferi a bassa permeabilità (a) e ad alta permeabilità (b).

The statistical analysis of the analytical solution developed by Ghyben (1888), Glover (1959), Rumer Jr & Harleman (1963), Verruijt (1968), and Kashef (1983), when compared with the numerical and experimental solution, revealed that, in most of the investigated cases, Rumer Jr & Harleman's equation was the most suitable choice with a minimum of the root mean square error (RMSE) in the calculated saltwater wedge length. The second-to-best equation was Kashef's equation (1983) (Appendix A).

In the low K aquifer, Lu et al. (2015) equation overestimates the toe length value by about 19.9% higher than the observed experimental steady-state data. The root mean square error (RMSE) equals 5.21 cm and the average significant correlation coefficient (R^2) equals 0.9997. In the high K aquifer, Lu et al. (2015) equation overestimates the toe length value by about 19.0% higher than the observed experimental steady-state data. The root mean square error (RMSE) equals 4.90 cm and the average significant correlation coefficient (R^2) equals 0.9990. On the other hand, the analytical values of saltwater toe length obtained by Anderson (2021) agreed well with the observed experimental saltwater toe length, with an average significant correlation coefficient (R^2) equal to 0.9990 and 0.9994 and RMSE equal to 0.54 and 1.77 cm for the low K and high K aquifers, respectively. The study revealed how SLR and inland water heads affect seawater intrusion characteristics under steady-state and transient conditions.

In future research, sensitivity analyses could be conducted to determine the model's sensitivity to changes in other input parameters or boundary conditions and the aquifer's heterogeneity should be addressed.

Acknowledgments

The authors would like to express their gratitude and recognition to the reviewers for their precious time and dedication to revising the manuscript.

Funding source

The authors declare that no funds, grants, or other support were received during the preparation of this manuscript.

Competing interest

The authors declare no competing interest.

Author contributions

This paper originated as a part of the PhD thesis of the first author (Sobhy R. Emara) under the supervision of Asaad M. Armanuos, Tamer A. Gado, and Bakenaz A. Zeidan. All authors contributed to the study conception and design. Sobhy R. Emara and Asaad M. Armanuos carried out the experiments. Sobhy R. Emara carried out the simulations. All authors contributed to the interpretation of the results. The first draft of the manuscript was written by Sobhy R. Emara. And all authors commented on previous versions of the manuscript. All authors have read and agreed to the final version of the manuscript.

Additional information

Supplementary information is available for this paper at <https://doi.org/10.7343/as-2023-668>

Reprint and permission information are available writing to acquessotterranee@anipapozzi.it

Publisher's note Associazione Acque Sotterranee remains neutral with regard to jurisdictional claims in published maps and institutional affiliations.

REFERENCES

- Abarca, E., & Clement, T. P. (2009). A novel approach for characterizing the mixing zone of a saltwater wedge. *Geophysical Research Letters*, 36(6). <https://doi.org/10.1029/2008GL036995>
- Abd-Elaty, I., & Zelenakova, M. (2022). Saltwater intrusion management in shallow and deep coastal aquifers for high aridity regions. *Journal of Hydrology: Regional Studies*, 40, 101026. <https://doi.org/10.1016/j.jhrh.2022.101026>
- Abd-Elhamid, H. F., Abd-Elaty, I., & Hussain, M. S. (2020). Mitigation of seawater intrusion in coastal aquifers using coastal earth fill considering future sea level rise. *Environmental Science and Pollution Research*, 27(18), 23234–23245. <https://doi.org/10.1007/s11356-020-08891-1>
- Abdoulhalik, A., & Ahmed, A. A. (2017). The effectiveness of cutoff walls to control saltwater intrusion in multi-layered coastal aquifers: Experimental and numerical study. *Journal of Environmental Management*, 199, 62–73. <https://doi.org/10.1016/j.jenvman.2017.05.040>
- Abdoulhalik, A., & Ahmed, A. A. (2018). Transience of seawater intrusion and retreat in response to incremental water-level variations. *Hydrological Processes*, 32(17), 2721–2733. <https://doi.org/10.1002/hyp.13214>
- Abdoulhalik, A., Ahmed, A. A., Abdelgawad, A. M., & Hamill, G. A. (2021). Towards a Correlation between Long-Term Seawater Intrusion Response and Water Level Fluctuations. *Water*, 13(5), 719. <https://doi.org/10.3390/w13050719>
- Abdoulhalik, A., Ahmed, A., & Hamill, G. A. (2017). A new physical barrier system for seawater intrusion control. *Journal of Hydrology*, 549, 416–427. <https://doi.org/10.1016/j.jhydrol.2017.04.005>
- Anderson, E. I. (2021). Analytical Solutions for Confined and Unconfined Coastal Interface Flow by the Hodograph Method. *Water Resources Research*, 57(9). <https://doi.org/10.1029/2021WR030323>
- Armanuos, A. M., Al-Ansari, N., & Yaseen, Z. M. (2020a). Assessing the Effectiveness of Using Recharge Wells for Controlling the Saltwater Intrusion in Unconfined Coastal Aquifers with Sloping Beds: Numerical Study. *Sustainability*, 12(7), 2685. <https://doi.org/10.3390/su12072685>
- Armanuos, A. M., Al-Ansari, N., & Yaseen, Z. M. (2020b). Underground Barrier Wall Evaluation for Controlling Saltwater Intrusion in Sloping Unconfined Coastal Aquifers. *Water*, 12(9), 2403. <https://doi.org/10.3390/w12092403>
- Armanuos, A. M., Ibrahim, M. G., Mahmud, W. E., Takemura, J., & Yoshimura, C. (2019). Analysing the Combined Effect of Barrier Wall and Freshwater Injection Countermeasures on Controlling Saltwater Intrusion in Unconfined Coastal Aquifer Systems. *Water Resources Management*, 33(4), 1265–1280. <https://doi.org/10.1007/s11269-019-2184-9>
- Brakefield, L. (2008). Physical and Numerical Modeling of Buoyant Groundwater Plumes [Thesis]. <https://etd.auburn.edu/handle/10415/1038>
- Chang, Q., Zheng, T., Chen, Y., Zheng, X., & Walther, M. (2020). Investigation of the elevation of saltwater wedge due to subsurface dams. *Hydrological Processes*, 34(22), 4251–4261. <https://doi.org/10.1002/hyp.13863>
- Chang, Q., Zheng, T., Zheng, X., Zhang, B., Sun, Q., & Walther, M. (2019). Effect of subsurface dams on saltwater intrusion and fresh groundwater discharge. *Journal of Hydrology*, 576, 508–519. <https://doi.org/10.1016/j.jhydrol.2019.06.060>
- Chang, S. W., Clement, T. P., Simpson, M. J., & Lee, K.-K. (2011). Does sea-level rise have an impact on saltwater intrusion? *Advances in Water Resources*, 34(10), 1283–1291. <https://doi.org/10.1016/j.advwatres.2011.06.006>
- Christensen, B., & JR, E. A. (1974). A physical model for prediction and control of saltwater intrusion in the Floridan aquifer. University of Florida. Water Resources Research Center, Gainesville, Fa, 88.

- Dang, N. M., Vien, L. N., Tung, N. B., Duong, T. A., & Dang, T. D. (2020). Assessments of Climate Change and Sea Level Rise Impacts on Flows and Saltwater Intrusion in the Vu Gia—Thu Bon River Basin, Vietnam. In N. Trung Viet, D. Xiping, & T. Thanh Tung (Eds.), *APAC 2019* (pp. 1367–1374). Springer Singapore. https://doi.org/10.1007/978-981-15-0291-0_185
- Diersch, H.-J. G. (2013). FEFLOW—Finite Element Modeling of Flow, Mass and Heat Transport in Porous and Fractured Media. In *FEFLOW: Finite Element Modeling of Flow, Mass and Heat Transport in Porous and Fractured Media* (p. 996). <https://doi.org/10.1007/978-3-642-38739-5>
- Fang, Y., Zheng, T., Guo, B., Zhan, H., Wang, H., Zheng, X., & Walther, M. (2022). Transformation in the Stability of Tide-Induced Upper Saline Plume Driven by Transient External Forcing. *Water Resources Research*, 58(6), e2021WR031331. <https://doi.org/10.1029/2021WR031331>
- Gao, M., Zheng, T., Chang, Q., Zheng, X., & Walther, M. (2021). Effects of mixed physical barrier on residual saltwater removal and groundwater discharge in coastal aquifers. *Hydrological Processes*, 35(7). <https://doi.org/10.1002/hyp.14263>
- Ghyben, B. W. (1888). Nota in verband met de voorgenomen putboring nabij, Amsterdam. The Hague, 21.
- Glover, R. E. (1959). The pattern of fresh-water flow in a coastal aquifer. *Journal of Geophysical Research*, 64(4), 457–459.
- Gossel, W., Sefelnasr, A., & Wycisk, P. (2010). Modelling of paleo-saltwater intrusion in the northern part of the Nubian Aquifer System, Northeast Africa. *Hydrogeology Journal*, 18(6), 1447–1463. <https://doi.org/10.1007/s10040-010-0597-x>
- Goswami, R. R., & Clement, T. P. (2007). Laboratory-scale investigation of saltwater intrusion dynamics. *Water Resources Research*, 43(4). <https://doi.org/10.1029/2006WR005151>
- Guo, Q., Zhang, Y., Zhou, Z., & Zhao, Y. (2020). Saltwater Transport under the Influence of Sea-Level Rise in Coastal Multilayered Aquifers. *Journal of Coastal Research*, 36(5), 1040. <https://doi.org/10.2112/JCOASTRES-D-19-00189.1>
- Guo, W., & Langevin, C. D. (2002). User's guide to SEAWAT; a computer program for simulation of three-dimensional variable-density ground-water flow.
- Herzberg, A. (1901). Die wasserversorgung einiger Nordseebader. *J. Gasbeleucht. Wasserversorg.*, 44, 842–844.
- Hussain, M. S., Abd-Elhamid, H. F., Javadi, A. A., & Sherif, M. M. (2019). Management of Seawater Intrusion in Coastal Aquifers: A Review. *Water*, 11(12), 2467. <https://doi.org/10.3390/w11122467>
- Kashef, A.-A. I. (1983). Harmonizing Ghyben-Herzberg interface with rigorous solutions. *Groundwater*, 21(2), 153–159.
- Ketabchi, H., Mahmoodzadeh, D., Ataie-Ashtiani, B., & Simmons, C. T. (2016). Sea-level rise impacts on seawater intrusion in coastal aquifers: Review and integration. *Journal of Hydrology*, 535, 235–255. <https://doi.org/10.1016/j.jhydrol.2016.01.083>
- Ketabchi, H., Mahmoodzadeh, D., Ataie-Ashtiani, B., Werner, A. D., & Simmons, C. T. (2014). Sea-level rise impact on fresh groundwater lenses in two-layer small islands. *Hydrological Processes*, 28(24), 5938–5953. <https://doi.org/10.1002/hyp.10059>
- Koussis, A. D., Mazi, K., & Destouni, G. (2012). Analytical single-potential, sharp-interface solutions for regional seawater intrusion in sloping unconfined coastal aquifers, with pumping and recharge. *Journal of Hydrology*, 416–417, 1–11. <https://doi.org/10.1016/j.jhydrol.2011.11.012>
- Kuan, W. K., Jin, G., Xin, P., Robinson, C., Gibbes, B., & Li, L. (2012). Tidal influence on seawater intrusion in unconfined coastal aquifers. *Water Resources Research*, 48(2). <https://doi.org/10.1029/2011WR010678>
- Lu, C., Xin, P., Kong, J., Li, L., & Luo, J. (2016). Analytical solutions of seawater intrusion in sloping confined and unconfined coastal aquifers. *Water Resources Research*, 52(9), 6989–7004. <https://doi.org/10.1002/2016WR019101>
- Lu, C., Xin, P., Li, L., & Luo, J. (2015). Seawater intrusion in response to sea-level rise in a coastal aquifer with a general-head inland boundary. *Journal of Hydrology*, 522, 135–140. <https://doi.org/10.1016/j.jhydrol.2014.12.053>
- Luo, Z., Kong, J., Shen, C., Lu, C., Xin, P., Werner, A. D., Li, L., & Barry, D. A. (2022). Approximate analytical solutions for assessing the effects of unsaturated flow on seawater extent in thin unconfined coastal aquifers. *Advances in Water Resources*, 160, 104104. <https://doi.org/10.1016/j.advwatres.2021.104104>
- Luyun Jr, R., Momii, K., & Nakagawa, K. (2011). Effects of recharge wells and flow barriers on seawater intrusion. *Groundwater*, 49(2), 239–249. <https://doi.org/10.1111/j.1745-6584.2010.00719.x>
- Mehdizadeh, S. S., Karamalipour, S. E., & Asoodeh, R. (2017). Sea level rise effect on seawater intrusion into layered coastal aquifers (simulation using dispersive and sharp-interface approaches). *Ocean & Coastal Management*, 138, 11–18. <https://doi.org/10.1016/j.ocecoaman.2017.01.001>
- Rumer Jr, R. R., & Harleman, D. R. (1963). Intruded salt-water wedge in porous media. *Journal of the Hydraulics Division*, 89(6), 193–220.
- Sherif, M., Sefelnasr, A., Ebraheem, A. A., & Javadi, A. (2014). Quantitative and Qualitative Assessment of Seawater Intrusion in Wadi Ham under Different Pumping Scenarios. *Journal of Hydrologic Engineering*, 19(5), 855–866. [https://doi.org/10.1061/\(ASCE\)HE.1943-5584.0000907](https://doi.org/10.1061/(ASCE)HE.1943-5584.0000907)
- Shi, W., Lu, C., Ye, Y., Wu, J., Li, L., & Luo, J. (2018). Assessment of the impact of sea-level rise on steady-state seawater intrusion in a layered coastal aquifer. *Journal of Hydrology*, 563, 851–862. <https://doi.org/10.1016/j.jhydrol.2018.06.046>
- Song, Z., Shi, W., Zhang, J., Yuan, D., Wu, Q., & Wang, R. (2020). Impact of sea level rise on estuarine salt water intrusion—A numerical model study for Changjiang Estuarine. *IOP Conference Series: Earth and Environmental Science*, 525, 012130. <https://doi.org/10.1088/1755-1315/525/1/012130>
- Sriapai, T., Walsri, C., Phueakphum, D., & Fuenkajorn, K. (2012). Physical model simulations of seawater intrusion in unconfined aquifer. *Songklanakarin Journal of Science & Technology*, 34(6).
- Sun, Q., Zheng, T., Zheng, X., Chang, Q., & Walther, M. (2019). Influence of a subsurface cut-off wall on nitrate contamination in an unconfined aquifer. *Journal of Hydrology*, 575, 234–243. <https://doi.org/10.1016/j.jhydrol.2019.05.030>
- Verruijt, A. (1968). A note on the Ghyben-Herzberg formula. *Hydrological Sciences Journal*, 13(4), 43–46.
- Voss, A., & Koch, M. (2001). Numerical simulations of topography-induced saltwater upconing in the state of Brandenburg, Germany. *Physics and Chemistry of the Earth, Part B: Hydrology, Oceans and Atmosphere*, 26(4), 353–359. [https://doi.org/10.1016/S1464-1909\(01\)00018-1](https://doi.org/10.1016/S1464-1909(01)00018-1)
- Voss, C. I., & Souza, W. R. (1987). Variable density flow and solute transport simulation of regional aquifers containing a narrow freshwater-saltwater transition zone. *Water Resources Research*, 23(10), 1851–1866. <https://doi.org/10.1029/WR023i010p01851>
- Vu, D. T., Yamada, T., & Ishidaira, H. (2018). Assessing the impact of sea level rise due to climate change on seawater intrusion in Mekong Delta, Vietnam. *Water Science and Technology*, 77(6), 1632–1639. <https://doi.org/10.2166/wst.2018.038>
- Walther, M., Graf, T., Kolditz, O., Liedl, R., & Post, V. (2017). How significant is the slope of the sea-side boundary for modelling seawater intrusion in coastal aquifers? *Journal of Hydrology*, 551, 648–659. <https://doi.org/10.1016/j.jhydrol.2017.02.031>
- Werner, A. D., Bakker, M., Post, V. E. A., Vandenbohede, A., Lu, C., Ataie-Ashtiani, B., Simmons, C. T., & Barry, D. A. (2013). Seawater intrusion processes, investigation and management: Recent advances and future challenges. *Advances in Water Resources*, 51, 3–26. <https://doi.org/10.1016/j.advwatres.2012.03.004>
- Zheng, T., Zheng, X., Chang, Q., Zhan, H., & Walther, M. (2021). Timescale and Effectiveness of Residual Saltwater Desalination Behind Subsurface Dams in an Unconfined Aquifer. *Water Resources Research*, 57(2), e2020WR028493. <https://doi.org/10.1029/2020WR028493>